NOXA expression drives synthetic lethality to RUNX1 inhibition in pancreatic cancer

Josefina Doffo[a], Stefanos A. Bamopoulos[a], Hazal Köse[a], Felix Orben[b], Chuanbing Zang[a], Miriam Pons[c], Alexander T. den Dekker[d,e], Rutger W. W. Brouwer[d,e], Apoorva Baluapuri[f], Stefan Habringer[a], Maximillian Reichert[b], Anuradha Illendula[g], Oliver H. Krämer[c], Markus Schick[a], Elmar Wolf[f], Wilfred F. J. van IJcken[d,e], Irene Esposito[h], Ulrich Keller[a,i,j,k], Günter Schneider[c,i,k,l], and Matthias Wirth[a,1]

[a]Department of Hematology, Oncology and Cancer Immunology, Charité - Universitätsmedizin Berlin, Freie Universität Berlin and Humboldt-Universität zu Berlin, 10117 Berlin, Germany; [b]Department of Medicine II (Gastroenterology and GI Oncology), Klinikum Rechts der Isar, School of Medicine, Technische Universität München, 81675 München, Germany; [c]Department of Toxicology, University Medical Center, 55131 Mainz, Germany; [d]Center for Biomics, Erasmus University Medical Center, 3015 GD Rotterdam, The Netherlands; [e]Department of Cell Biology, Erasmus University Medical Center, 3015 GD Rotterdam, The Netherlands; [f]Cancer Systems Biology Group, Department of Biochemistry and Molecular Biology, Biocenter, University of Würzburg, 97070 Würzburg, Germany; [g]Department of Pharmacology, University of Virginia, Charlottesville, VA 22903; [h]Institute of Pathology, Heinrich Heine University and University Hospital of Düsseldorf, 40225 Düsseldorf, Germany; [i]German Cancer Research Center, 69120 Heidelberg, Germany; [j]German Cancer Consortium, 69120 Heidelberg, Germany; [k]Max-Delbrück-Center for Molecular Medicine, 13125 Berlin, Germany; and [l]Department of General, Visceral and Pediatric Surgery, University Medical Center Göttingen, 37075 Göttingen, Germany

Edited by Nancy Speck, Department of Cell and Developmental Biology, Raymond and Ruth Perelman School of Medicine at the University of Pennsylvania, Philadelphia, PA; received March 24, 2021; accepted November 23, 2021

Evasion from drug-induced apoptosis is a crucial mechanism of cancer treatment resistance. The proapoptotic protein NOXA marks an aggressive pancreatic ductal adenocarcinoma (PDAC) subtype. To identify drugs that unleash the death-inducing potential of NOXA, we performed an unbiased drug screening experiment. In *NOXA*-deficient isogenic cellular models, we identified an inhibitor of the transcription factor heterodimer CBFβ/RUNX1. By genetic gain and loss of function experiments, we validated that the mode of action depends on RUNX1 and NOXA. Of note is that RUNX1 expression is significantly higher in PDACs compared to normal pancreas. We show that pharmacological RUNX1 inhibition significantly blocks tumor growth in vivo and in primary patient-derived PDAC organoids. Through genome-wide analysis, we detected that *RUNX1*-loss reshapes the epigenetic landscape, which gains H3K27ac enrichment at the *NOXA* promoter. Our study demonstrates a previously unknown mechanism of NOXA-dependent cell death, which can be triggered pharmaceutically. Therefore, our data show a way to target a therapy-resistant PDAC, an unmet clinical need.

NOXA | apoptosis | PDAC | RUNX1 | pancreatic cancer

Pancreatic ductal adenocarcinoma (PDAC) is an aggressive disease often diagnosed at an advanced stage. The incidence of PDAC is steadily increasing, and PDAC is predicted to be the second leading cause of cancer-related death by 2030 (1). Evasion of apoptosis is a characteristic of PDAC and is often associated with treatment resistance (2, 3). A dysregulated transcription commonly results in apoptosis resistance (4). Therefore, the identification of novel concepts to reactivate apoptosis by disrupting cancerous transcription programs is a promising approach for the effective elimination of PDAC cells (3, 5).

Comprehensive integrated genome analyses from RNA expression profiles in recent years revealed different subtypes of PDAC with variable biology and therapeutic responsiveness (6–9). *NOXA* (Latin for damage; also known as PMAIP1 [Phorbol-12-myristate-13-acetate-induced protein 1]) is part of an identifier gene set for the quasi-mesenchymal (QM) subtype of the disease (8). This subtype overlaps with the described basal-like and squamous subtype of the disease, which is particularly resistant to the currently used chemotherapeutics (7, 9).

NOXA belongs to the BCL-2 homology (BH) BH3-only subgroup of the B cell lymphoma 2 (BCL2) protein family which is essential for the regulation of cell intrinsic apoptosis (10). BCL2 proteins are divided into sensor, effector, and protector proteins (10). The classical antiapoptotic protector proteins, including Myeloid cell leukemia 1 (MCL1), inhibit effector proteins (e.g., BCL-2–associated X protein), thereby blocking apoptosis. Proapoptotic sensor proteins, including NOXA, which directly binds to MCL1, neutralize the antiapoptotic function of the protector proteins (10), leading to the initiation of apoptotic cell death. In PDAC, *NOXA* is tightly regulated at the transcriptional level, and transcriptional activation of *NOXA* by HDAC inhibitors or proteasome inhibitors contributes to induce the cell intrinsic apoptosis pathway (11–13). Furthermore, *NOXA* is regulated by multiple transcription factors, including p53, and is involved in apoptosis under genotoxic stress (14, 15).

Runt-related (RUNX) proteins are master regulators involved in a broad range of biological processes, including

Significance

Recent evidence demonstrated the existence of molecular subtypes in pancreatic ductal adenocarcinoma (PDAC), which resist all current therapies. The paucity of therapeutic options, including a complete lack of targeted therapies, underscores the urgent and unmet medical need for the identification of targets and novel treatment strategies for PDAC. Our study unravels a function of the transcription factor RUNX1 in apoptosis regulation in PDAC. We show that pharmacological RUNX1 inhibition in PDAC is feasible and leads to NOXA-dependent apoptosis. The development of targeted therapies that influence the transcriptional landscape of PDAC might have great benefits for patients who are resistant to conventional therapies. RUNX1 inhibition as a new therapeutic intervention offers an attractive strategy for future therapies.

Author contributions: O.H.K., W.F.J.v.I., G.S., and M.W. designed research; J.D., H.K., F.O., C.Z., M.P., A.T.d.D., R.W.W.B., A.B., and M.W. performed research; M.R., E.W., W.F.J.v.I., I.E., U.K., and G.S. contributed new reagents/analytic tools; J.D., S.A.B., C.Z., A.T.d.D., R.W.W.B., A.B., and M.W. analyzed data; and J.D., S.A.B., S.H., A.I., O.H.K., M.S., E.W., W.F.J.v.I., I.E., U.K., G.S., and M.W. wrote the paper.

The authors declare no competing interest.

This article is a PNAS Direct Submission.

[1]To whom correspondence may be addressed. Email: matthias.wirth@charite.de.

This article contains supporting information online at http://www.pnas.org/lookup/suppl/doi:10.1073/pnas.2105691119/-/DCSupplemental.

Published February 23, 2021.

proliferation, differentiation, and apoptosis (16). DNA binding of these transcription factors is mediated by heterodimerization of a core DNA binding factor alpha chain (CBFα), composed of one of the three RUNX family members, RUNX1 to RUNX3, to the non-DNA binding core binding factor beta (CBFβ). Each of the three RUNX family members plays important roles in different stages of tumor development (17). As has been shown in mouse models, knockouts of any of the three RUNX transcription factors exhibit significant developmental defects: RUNX1 plays an important role in hematopoiesis (18), RUNX2 plays an important role in bone development (19), and RUNX3 plays an important role in the gastrointestinal tract (20) and in neurogenesis (21). RUNX expression patterns are highly dynamic and depend on the stage of differentiation, development, and environmental conditions (22). In addition, RUNX transcription factors are expressed in almost all cancers (23). Besides its implication in leukemogenesis (24), RUNX1 is strongly expressed in a broad spectrum of solid tumors (25) and is associated with poor prognosis in PDAC (26). Depending on the cellular context, RUNX1 can act both oncogenic and tumor suppressive in solid tumors (27). RUNX1 interacts with various cofactors to shape gene expression. RUNX1-dependent activation of target genes is mediated through an interaction with CBP/p300 (28) and the protein arginine methyltransferase 1 (PRMT1) (29). The inhibitory function of RUNX1 is achieved by interaction with corepressors such as the Sin3A–HDAC corepressor complex (30).

In this study, we aimed at identifying strategies affecting the delicate balance of NOXA expression to drive cell death in an aggressive subtype of PDAC. We found that inhibition of RUNX1 led to a global gain of H3K27ac enrichment contributing to the activation of the proximal *NOXA* promoter region, and we suggest a strategy to overcome treatment resistance in an aggressive subtype of PDAC with inferior prognosis.

Materials and Methods

Cell Culture and Cell Viability Assay. Cell lines were cultured in Dulbecco's Modified Eagle's Medium (Thermo Fisher Scientific, #41965062) or Roswell Park Memorial Institute 1640 Medium (Thermo Fisher Scientific, #21875091) supplemented with 10% fetal bovine serum (Thermo Fisher Scientific, #10270106) and 1% penicillin/streptomycin (Thermo Fisher Scientific, #15070063). They were passaged up to 14 times in a 1:10 dilution every 3 d to 4 d. Murine PDAC cell lines were generated from *Kras*^{G12D}-driven mouse models as described (13). For all cell lines used, PCR-based mycoplasma tests were performed at regular intervals. Cell viability was measured by MTT-Test (Sigma-Aldrich, #M5655). Detailed information on the procedures for cell viability, drug screening, and colony formation assay are provided in *SI Appendix, Supplementary Materials and Methods*.

Patient-Derived Organoids. PDAC biopsies and tissues were received from endoscopy punctures or surgical resection. Three-dimensional organoids were collected, propagated, and analyzed in agreement with the declaration of Helsinki. This study was approved by the ethical committee of the Technical University of Munich (TUM) (Project 207/15). Written informed consent from the patients for research use of tumor material was obtained prior to the use. Detailed information is provided in *SI Appendix, Supplementary Materials and Methods*.

In Vivo Drug Efficacy Analysis in Mice and Immunohistochemistry. Xenograft assays were performed by Experimental Pharmacology and Oncology, Berlin-Buch. All animal experiments were approved by the local responsible authorities and performed in accordance with the German Animal Protection law. Detailed information is provided in *SI Appendix, Supplementary Materials and Methods*.

Statistical Analysis, Quantitative Chromatin Immunoprecipitation, Chromatin Immunoprecipitation DNA-Sequencing, RNA-Sequencing, Assay for Transposase-Accessible Chromatin Using Sequencing, Chromosome Conformation Capture-on-Chip, Quantitative PCR, Western Blot, and CRISPR Editing. Detailed information on the procedures and data analyses are provided in *SI Appendix, Supplementary Materials and Methods* and Table S6.

Results

High *NOXA* mRNA Expression Is Associated with an Aggressive PDAC Subtype. As a stress response, tumor cells may express proapoptotic effectors that can be neutralized by antiapoptotic counterparts, thus dampening the apoptotic response. Such tumor cells expose apoptotic potential. To investigate whether classical proapoptotic BH3-only proteins may contribute to this phenotype, we analyzed the messenger RNA (mRNA) expression of BH3-only genes (6) and filtered for transcriptome profiles of human PDAC tumors (Fig. 1*A*). From these data, we extracted indicated classical BH3-only genes, performed a hierarchical clustering based on the mRNA expression of the BH3-only genes, and subdivided PDAC patient samples into the squamous subtype and combined the ADEX, classical, and immunogenic subtypes as "other" subtypes. We subsequently determined whether the mRNAs of the listed classical BH3-only members are significantly enriched in these two groups. Of note is that specifically high expression of *NOXA* was significantly ($P < 0.001$) associated with the squamous subtype (Fig. 1*A* and *SI Appendix*, Fig. S1*A*), which is in line with the described expression in QM cancers (8). In accordance with this finding, high *NOXA* expression (>75th percentile) characterized a PDAC patient cohort with inferior survival as compared to patients with low *NOXA* expression (<25th percentile) in International Cancer Genome Consortium (ICGC)/Bailey et al. (6) (Fig. 1*B* and *SI Appendix*, Fig. S1*B*) and The Cancer Genome Atlas (TCGA) datasets (*SI Appendix*, Fig. S1*C*). In addition, we analyzed transcriptome profiles of a larger set of patients ($n = 248$), allowing fine-tuning of PDAC subtyping into A and B subsets of the basal-like and classical-like subtypes (31). Here, we confirmed that *NOXA* had a significantly increased expression in basal-like A and basal-like B subtypes compared to classical subtypes A and B (Fig. 1*C*).

We hypothesized that the high expression of *NOXA* indicates that these tumors harbor an apoptotic potential, and that shifting the balance of apoptosis regulators to a proapoptotic state may constitute a therapeutic strategy.

Identification of a Synthetic Lethal Interaction of NOXA and Inhibition of RUNX1. By analyzing transcriptome profiles, we selected human PDAC cell lines of the QM subtype (8) (*SI Appendix*, Fig. S1*D*) and Kras^{G12D}-driven murine PDAC cell lines that exhibit relatively high basal *Noxa* mRNA expression (*SI Appendix*, Fig. S1*E*) for cross-species validation to identify drugs that affect the apoptotic balance. To investigate vulnerabilities specifically created by NOXA expression, we generated human and murine isogenic PDAC cell line models with genetically defined NOXA status (*SI Appendix*, Fig. S2 *A–D*). To prove *NOXA* deficiency, we performed Western blotting of the two human PDAC cell lines PSN1 and MiaPaCa-2. NOXA protein was absent in *NOXA*^{ko} cell lines (Fig. 1*D*). Importantly, *NOXA* deficiency did not influence the proliferation of the isogeneic cell lines (Fig. 1*E*).

To identify vulnerabilities associated with NOXA, we next performed a drug screening with a total of 1,842 compounds in *NOXA*-proficient (parental) and *NOXA*-deficient (*NOXA*^{ko}) cells and measured viability (Fig. 1*F*). Drug testing and viability assays were performed with a single concentration of 600 nM, as previously described (13). For identification of effects due of the NOXA status, we used a cutoff of 10% difference in viability (Fig. 1*G*). Out of the 1,842 compounds, we identified 50 drugs that showed higher efficiency in parental cell lines compared to *NOXA*^{ko} cell lines. Importantly, within the hits found, we identified topoisomerase and proteasome inhibitors, which is in line with data from previous studies (11–13), underlining the robustness of our screening experiment (*SI Appendix*, Table S1). From our screening hits, we selected for specific targeted molecules (target specificity) and novelty (Fig. 1*F*) and further validated 12 hits with

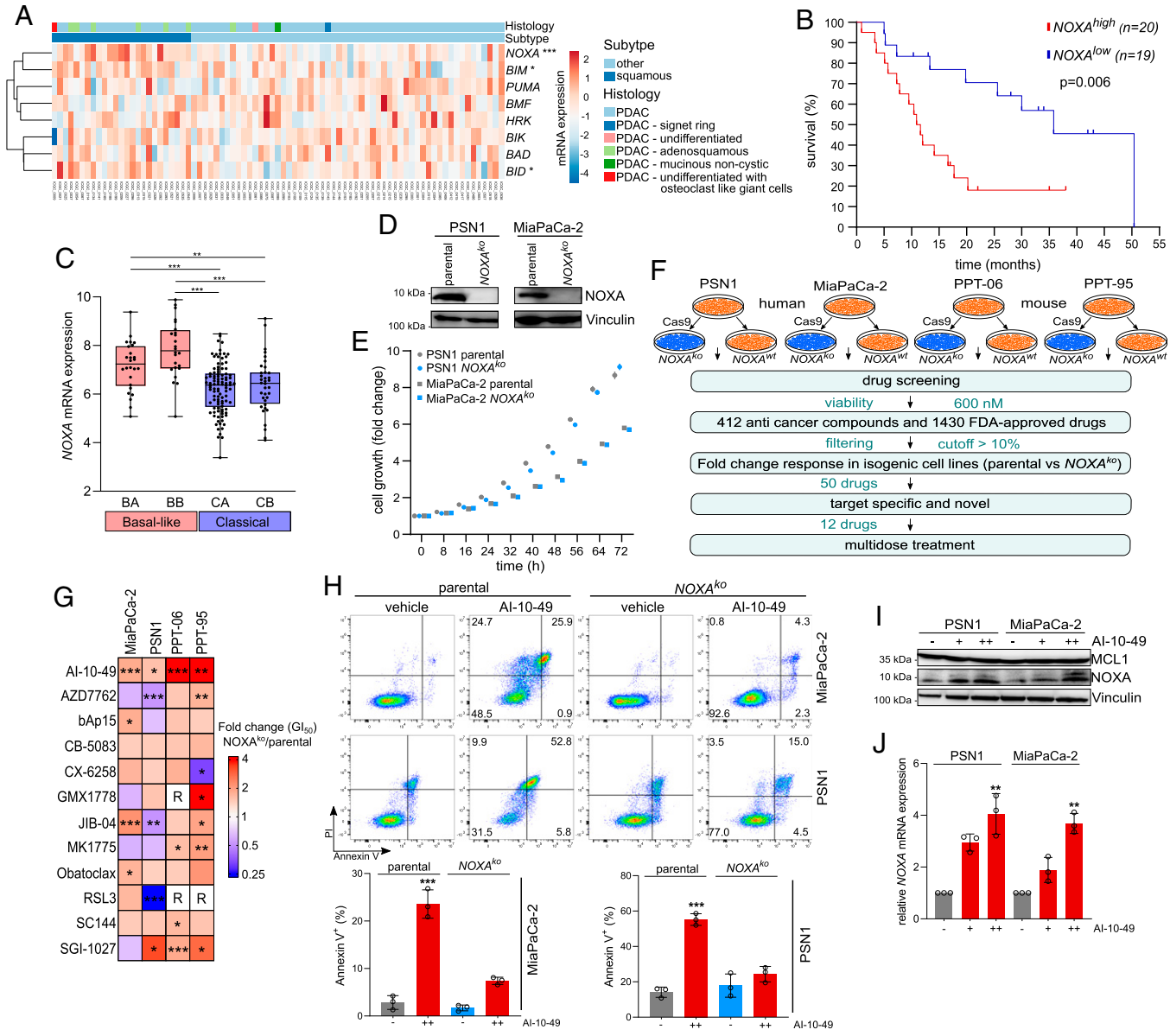

Fig. 1. Screening for NOXA-associated vulnerabilities in PDAC cells. (*A*) Cluster analysis of mRNA from classical BH3-only proteins, derived from transcriptome profiles of PDAC patients (6). Molecular subtypes have been divided into two groups: The aggressive squamous subtype and all other subtypes have been merged to others. Histological subtypes are indicated. Upper and lower quartiles of indicated mRNAs were identified. Significant (Fisher exact test) frequencies of a high mRNA expression of the indicated genes (upper quartile) in the squamous subtype are indicated (*$P < 0.05$, ***$P < 0.001$). (*B*) Survival of PDAC patients with a low (lower quartile) and a high (upper quartile) *NOXA* mRNA expression, derived from the dataset described in *A* (6). Log rank test: $P = 0.006$. (*C*) *NOXA* mRNA expression analysis in $n = 248$ PDAC patient samples (31), divided into classical A and B and basal-like A and B subtypes (Accession ID: EGAD00001006152). (*D*) Western blot analysis of NOXA protein in PSN1 and MiaPaCa-2 parental and isogenic *NOXA*^{ko} cell lines. Vinculin served as loading control. (*E*) Growth curves of PSN1 and MiaPaCa-2 parental and isogenic *NOXA*^{ko} cell lines performed with live-cell imaging. Five pictures per well were taken every 8 h, and growth was calculated as confluence (percent) normalized to 0-h control. (*F*) Schematic representation of the performed high-throughput drug screening strategy. Four human pancreatic cancer cell lines (two parental and two *NOXA*^{ko}) and four murine cell lines (two parental and two *NOXA*^{ko}) were used for screening a total of 1,842 drugs. These compounds were added to each cell line 24 h after seeding at a concentration of 600 nM, and cell viability was measured by MTT assay after 72 h; $n = 3$; all biological replicates were performed as technical triplicates. The inhibitors that differentially reduced viability in parental cell lines up to 10% more in comparison to *NOXA*^{ko} cells were further followed. Based on target treatment and or/novelty, 12 drugs were selected out of the first 50 hits. The GI_{50} of the drugs for murine and human cell lines was calculated from dose–response treatment using MTT assay. (*G*) Dose–response treatment in eight human and murine pancreatic cancer cell lines (four parental and four *NOXA*^{ko}). The fold change of the GI_{50} of the knockout cell lines compared to the parental is depicted; $n = 3$; all biological replicates were performed as technical triplicates. Red represents sensitivity in parental cell line in respect to its isogenic counterpart (smaller GI_{50}). Blue stands for higher sensitivity in the knockout cell line. R, resistant cell line within the used doses. Dose–response inhibition was calculated with logarithmic regression and tested for significance with logit model (*$P < 0.05$, **$P < 0.01$, ***$P < 0.001$). (*H*) FACS analysis of Annexin V/PI stained parental and *NOXA*^{ko} and cells after 72 h treatment with 3 μM AI-10-49 (++) or dimethyl sulfoxide (DMSO) (-) as vehicle control; $n = 3$; all biological replicates were performed as technical triplicates. *P* value of unpaired *t* test ***$P < 0.001$. (*I*) Western blot analysis of NOXA and MCL1 proteins in pancreatic cancer cell lines after 6 h AI-10-49 treatment. Representative Western blot is shown. Vinculin served as loading control; $n = 3$; all biological replicates were performed as technical triplicates. (-) DMSO, (+) 1.5 μM AI-10-49, (++) 3 μM AI-10-49. (*J*) The qPCR of *NOXA* in PSN1 and MiaPaCa-2 cell lines. (Conditions are as described in *H*).

multidose experiments (Fig. 1*G*). Only one of these 12 compounds analyzed in the validation experiments, AI-10-49, showed no growth inhibition in *NOXA*^{ko} cell lines, whereas viability of *NOXA*-proficient cells was dose-dependently reduced (Fig. 1*G*). AI-10-49 was originally designed to inhibit the interaction of the oncofusion protein CBFβ-SMMHC with RUNX1 (32). The lead compound of the bivalent AI-10-49 has been shown to inhibit RUNX1/CBFβ (33). Coimmunoprecipitations with either RUNX1 or CBFβ revealed AI-10-49 as a RUNX1/CBFβ inhibitor in MiaPaCa-2 cells (*SI Appendix*, Fig. S2*E*). Additionally, using the SwissTargetPrediction tool (34), CBFβ was a predicted target of this compound (*SI Appendix*, Table S2).

In summary, our data suggest that impairment of RUNX1 activity may affect NOXA-dependent execution of cell death in PDAC.

Induction of NOXA by CBFβ/RUNX1 Inhibition. To investigate whether the AI-10-49–induced drop in viability is mediated by induction of the apoptotic process, we performed fluorometric analysis of Annexin V/PI stained PDAC cells. Indeed, the reduced viability in parental cell lines upon AI-10-49 treatment was clearly associated with a significant induction of cell death in parental cells, whereas only marginal apoptosis induction was observed in *NOXA*^{ko} cells (Fig. 1*H*).

We next investigated whether an altered expression of other BCL2 family members such as MCL1, BCL2, BCLx_L, BIM, BID, BAK, or BAX mediates AI-10-49–induced apoptosis. We detected PARP cleavage but did not detect differential expression of these BCL2 family proteins 6 and 24 h after AI-10-49 treatment (Fig. 1*I* and *SI Appendix*, Fig. S3 *A* and *B*); a marked induction of NOXA protein (Fig. 1*I*) and *NOXA* mRNA expression (Fig. 1*J*) was observed upon treatment with AI-10-49. In HCT116 cells harboring wild-type p53, a DNA damage stimulus induced both RUNX1 and p53 and activated p53 target genes, including *NOXA* (35). To test whether p53 is involved in AI-10-49–induced *NOXA* expression, we treated murine cell lines harboring either wild-type, mutant, or deleted p53 (*SI Appendix*, Fig. S3*C*) with AI-10-49 and the topoisomerase II inhibitor etoposide (*SI Appendix*, Fig. S3*D*). While *Noxa* induction was highest in wild-type p53 cells upon etoposide treatment, we observed a rather uniform induction of *Noxa* in each of these cell lines after AI-10-49 treatment (*SI Appendix*, Fig. S3*D*). Since p53 is mutated in the human PDAC cell lines PSN1 and MiaPaCa-2, we also analyzed the expression of the p53 family member p63, but did not detect significant regulation (*SI Appendix*, Fig. S3*E*). Both p63 and mutant p53 showed no difference in expression at early time points after treatment with AI-10-49, but they tended to show decreased expression after 48 and 72 h, respectively (*SI Appendix*, Fig. S3 *B* and *E*). Our data show that both p53^{mut} and RUNX1 are not induced upon AI-10-49 treatment (*SI Appendix*, Fig. S3 *B* and *E*). Conversely, we rather observed a decreased expression of RUNX1 after AI-10-49 treatment in MiaPaCa-2 and PSN1 cells (*SI Appendix*, Fig. S3*E*).

Next, to substantiate caspase-induced apoptosis, we examined AI-10-49 together with the pan-caspase inhibitor zVAD-FMK by Annexin V/PI fluorescence-activated cell sorter (FACS). Here, we observed a significant rescue in apoptosis induction (Annexin V^+/PI^- fraction) (*SI Appendix*, Fig. S3*F*). Both fractions, that is, Annexin V^+/PI^- and Annexin V^+/PI^+, remained unaffected in *NOXA*^{ko} cells, indicating the relevance of NOXA in cell death (*SI Appendix*, Fig. S3*F*).

To further investigate the role of NOXA in AI-10-49 induced cell death, we generated MiaPaCa-2 cells stably expressing the CRISPR activator (CRISPRa) dCas9-MS2-p65-HSF1 (MpH), and an established *NOXA* single-guide RNA to endogenously overexpress NOXA (*SI Appendix*, Figs. S2*E* and S3*G*). *NOXA*-CRISPRa cells phenocopied AI-10-49–treated cells in clonogenic assays, and, more importantly, *NOXA*-CRISPRa cell growth was drastically inhibited when treated with AI-10-49 (*SI Appendix*, Fig. S3 *H* and *I*).

Together, our data show that inhibition of RUNX1 by AI-10-49 induces *NOXA* mRNA and protein expression and thereby drives NOXA-dependent apoptosis.

RUNX1 Is Up-Regulated in Pancreatic Cancer and Suppresses *NOXA* Expression. Understanding the mode of action of drugs is critical for the implementation of patient stratification strategies. To address this question, we next investigated how AI-10-49 induces *NOXA* expression. Since AI-10-49 inhibits the interaction between CBFβ and a DNA binding α subunit encoded by RUNX proteins (16), we tested whether loss of RUNX expression affects NOXA expression in knockouts of all three *RUNX* genes, *RUNX1*, *RUNX2*, and *RUNX3*, in MiaPaCa-2 cells (*SI Appendix*, Fig. S2*F*). Remarkably, we observed an induction of *NOXA* mRNA solely in *RUNX1* knockout cells (Fig. 2*A*), arguing for a RUNX1-specific repression of the *NOXA* gene. We validated this effect by small interfering RNA (siRNA)-mediated *RUNX1* depletion in Panc1, AsPC1, and MiaPaCa-2 cells (*SI Appendix*, Fig. S4*A*). In addition to the induction of *NOXA* mRNA, we also observed a significant NOXA induction in *RUNX1*^{ko} cells at the protein level (Fig. 2*B*). To analyze whether *RUNX1*^{ko} cells have a growth disadvantage, we compared colony formation of *RUNX1*^{ko} cells to the parental cell line. Here, we observed significantly reduced formation of colonies (Fig. 2*C*), which phenocopied the effects observed in AI-10-49–treated cells (*SI Appendix*, Fig. S3 *H* and *I*). In addition, *RUNX1*^{ko} cells showed an increased cell death rate at basal levels, as demonstrated by Annexin V flow cytometry (Fig. 2*D*). To demonstrate the specificity of AI-10-49 in this context, we applied AI-10-49 in two *RUNX1*^{ko} clones as well as in *RUNX1* siRNA-treated MiaPaCa-2 cells. Although we did not observe a consistent effect in the *RUNX1* knockout clones, which is probably related to the difficult cultivation of these cells, the use of siRNA, on the other hand, showed reproducible effects equivalent to a doubling of the drug concentration required for 50% growth inhibition (GI_{50}) value, confirming the dependence on RUNX1 (*SI Appendix*, Fig. S4*B*). These genetic experiments identify RUNX1 as a negative regulator of *NOXA* gene expression.

To further investigate the relevance of RUNX1 in PDAC, we analyzed RUNX1 expression in human and murine datasets. We found that RUNX1 indeed is transcriptionally up-regulated in pancreatic cancer in all three datasets investigated (Fig. 2*E* and *SI Appendix*, Fig. S4*C*). In addition, RUNX1 was expressed in pancreatic cancer, whereas it was not detected in normal pancreas on the protein level (Fig. 2*F*). In premalignant $Kras^{G12D}$-driven murine pancreatic epithelial cells, *Runx1* mRNA (Fig. 2*G*) and RUNX1 target gene signatures (Fig. 2*H*) were significantly enriched compared to normal pancreatic epithelial cells, displaying specificity for RUNX1 expression in nonstromal tumor-initiating cells. During PDAC progression, RUNX1 expression is maintained. Suspecting a RUNX1-mediated repression of the *NOXA* gene, we reanalyzed the ICGC/Bailey et al. (6) and Collisson et al. (8) transcriptome datasets and, indeed, observed a negative correlation trend of *RUNX1* and *NOXA* expression in the squamous/QM PDAC subtype (*SI Appendix*, Fig. S4*D*). To investigate whether RUNX1 expression was the main contributing factor to NOXA expression, we performed a short hairpin RNA-mediated knockdown of *NOXA* in *RUNX1*^{ko} cells (*SI Appendix*, Fig. S4*E*). Congruent with our initial findings, the basal apoptosis rates were restored (*SI Appendix*, Fig. S4*F*).

Taken together, these data argue for a RUNX1-mediated repression of NOXA expression.

RUNX1 Inhibition Induces *NOXA* through Amplification of Active Chromatin Marks. To understand the immediate effect of AI-10-49 treatment, we performed RNA sequencing (RNAseq) analyses of

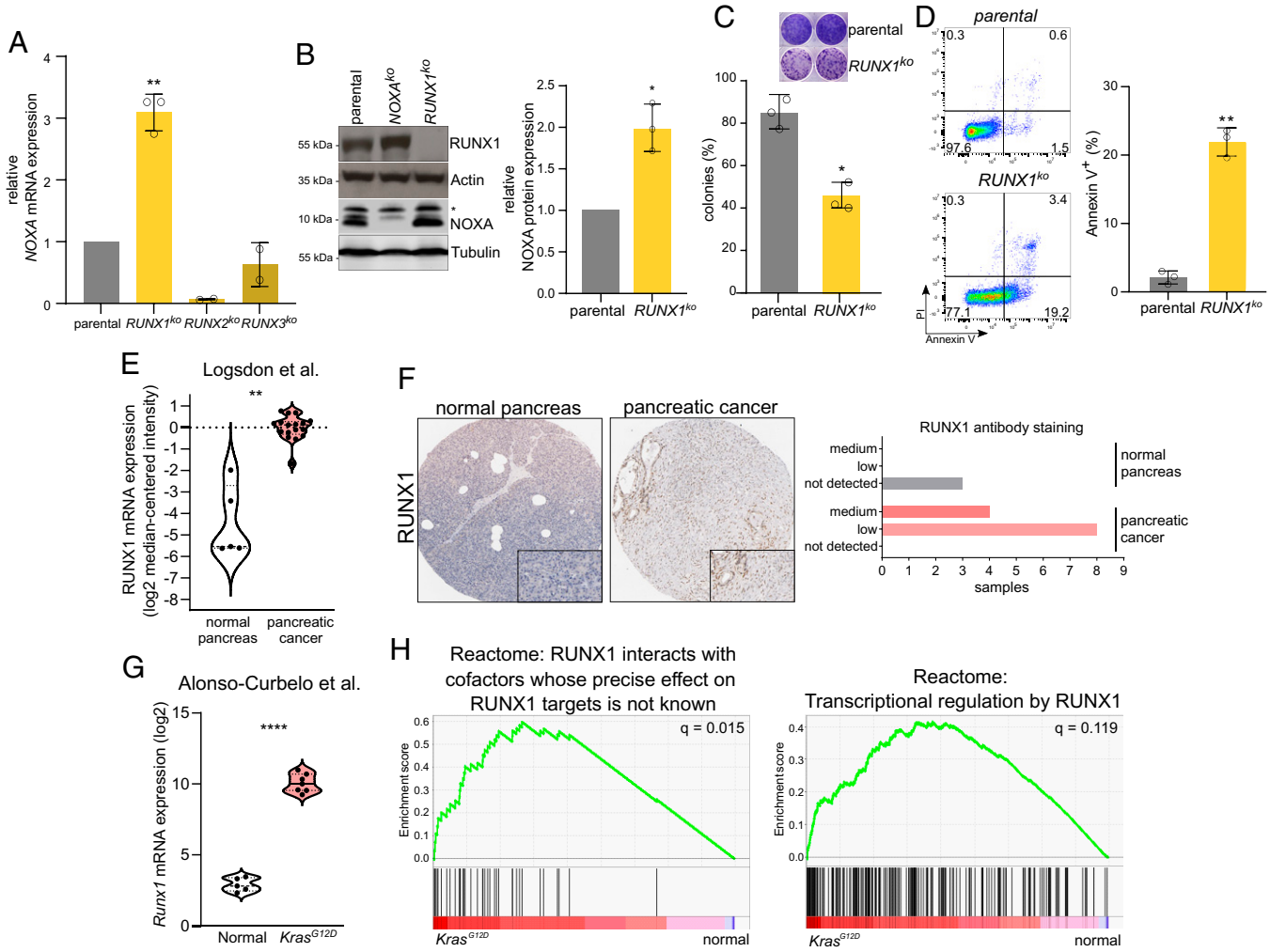

Fig. 2. RUNX1 is up-regulated in pancreatic cancer, and a genetic RUNX1 deletion induces NOXA transcription and apoptosis. (*A*) The qPCR of *NOXA* in parental, *RUNX1*^{ko}, *RUNX2*^{ko}, and *RUNX3*^{ko} MiaPaCa-2 cells. The mRNA fold change was calculated in comparison to parental cell line; $n = 3$; all biological replicates were performed as technical triplicates. $^{**}P < 0.01$. (*B*) Western blot analysis and quantification of NOXA and RUNX1 proteins in parental, *NOXA*^{ko}, and *RUNX1*^{ko} MiaPaCa-2 cells. Tubulin and actin served as loading controls. The asterisk (*) denotes an unspecific band. *P* value of *t* test, $P < 0.05$. (*C*) Representative image and quantification of clonogenic assay in parental and *RUNX1*^{ko} cells; $n = 3$; all biological replicates were performed as technical triplicates. *P* value of *t* test, $^{*}P < 0.05$. (*D*) FACS analysis of Annexin V stained parental and *RUNX1*^{ko} MiaPaCa-2 cells; $n = 3$; all biological replicates were performed as technical triplicates. *P* value of *t* test, $^{**}P < 0.01$. (*E*) *RUNX1* mRNA expression of patient samples from normal pancreas and pancreatic cancer (50), accessed via the oncomine.org, $^{**}P < 0.01$. (*F*) Immunohistochemistry (IHC) of patient samples from normal pancreas and pancreatic cancer accessed via the human protein atlas (51). Inset: Digital magnification of the section shown. (*G*) *RUNX1* mRNA expression of mouse samples from normal pancreatic epithelial cells and Kras^{G12D} pancreatic epithelial cells (52), $^{****}P < 0.0001$. (*H*) Gene set enrichment analysis (GSEA) of dataset, described in (52).

MiaPaCa2 cells 6 h after treatment in comparison to vehicle treated cells. Apart from NOXA, which was up-regulated in treated cells, less than 300 genes were found to be differentially expressed, suggesting a high specificity of AI-10-49 (Fig. 3*A*). Gene set enrichment analyses revealed a significant apoptosis signature and a negative enrichment score for RUNX1 targets (Fig. 3*B* and *SI Appendix*, Table S3) upon AI-10-49 treatment. To analyze the impact of RUNX1 inhibition on chromatin accessibility, we performed assays for transposase accessible chromatin with high-throughput sequencing (ATAC-seq). We observed reduced chromatin accessibility after AI-10-49 treatment, compared to the vehicle control 6 h after AI-10-49 treatment (Fig. 3*C*), and a redistribution of accessible consensus sequences (*SI Appendix*, Table S4).

To investigate the association of RUNX1 inhibition with regulation of chromatin dynamics, we performed H3K27ac ChIPseq experiments to detect transcriptionally active chromatin. A cross-coverage and fingerprint plot showed adequate signal strength in enriched regions (*SI Appendix*, Fig. S5 *A* and *B*). Globally, H3K27ac signal was increased in both replicates (Fig. 3*D* and *SI Appendix*, Fig. S5*C*), arguing for a neutralization of the repressor activity of RUNX1. Additionally, motif discovery analysis revealed that a redistribution of H3K27ac was observed after AI-10-49 treatment (*SI Appendix*, Table S4).

We also performed RUNX1 ChIPseq to assess the impact of RUNX1 inhibition on RUNX1 binding. This analysis showed a peak downstream of the *NOXA* gene, which we hypothesized to be an enhancer region and coined it "downstream binding site 1" (dBS1). To substantiate our findings, we analyzed RUNX1 ChIPseq from K562 and MCF10A cells. Indeed, we found an overlap of our identified peak in both ChIPseq datasets and were thus able to validate the peak identified in MiaPaCa-2 cells (*SI Appendix*, Fig. S6*A*). In both chromatin immunoprecipitation DNA sequencing (ChIPseq) and chromatin immunoprecipitation quantified by real-time PCR (qChIP) experiments, we observed a drop in RUNX1 binding at dBS1 and an increased acetylation of H3K27 at the *NOXA* promoter upon AI-10-49 treatment (Fig. 3 *E* and *F*), indicating an activation of the gene by acetylation of the proximal promoter region of

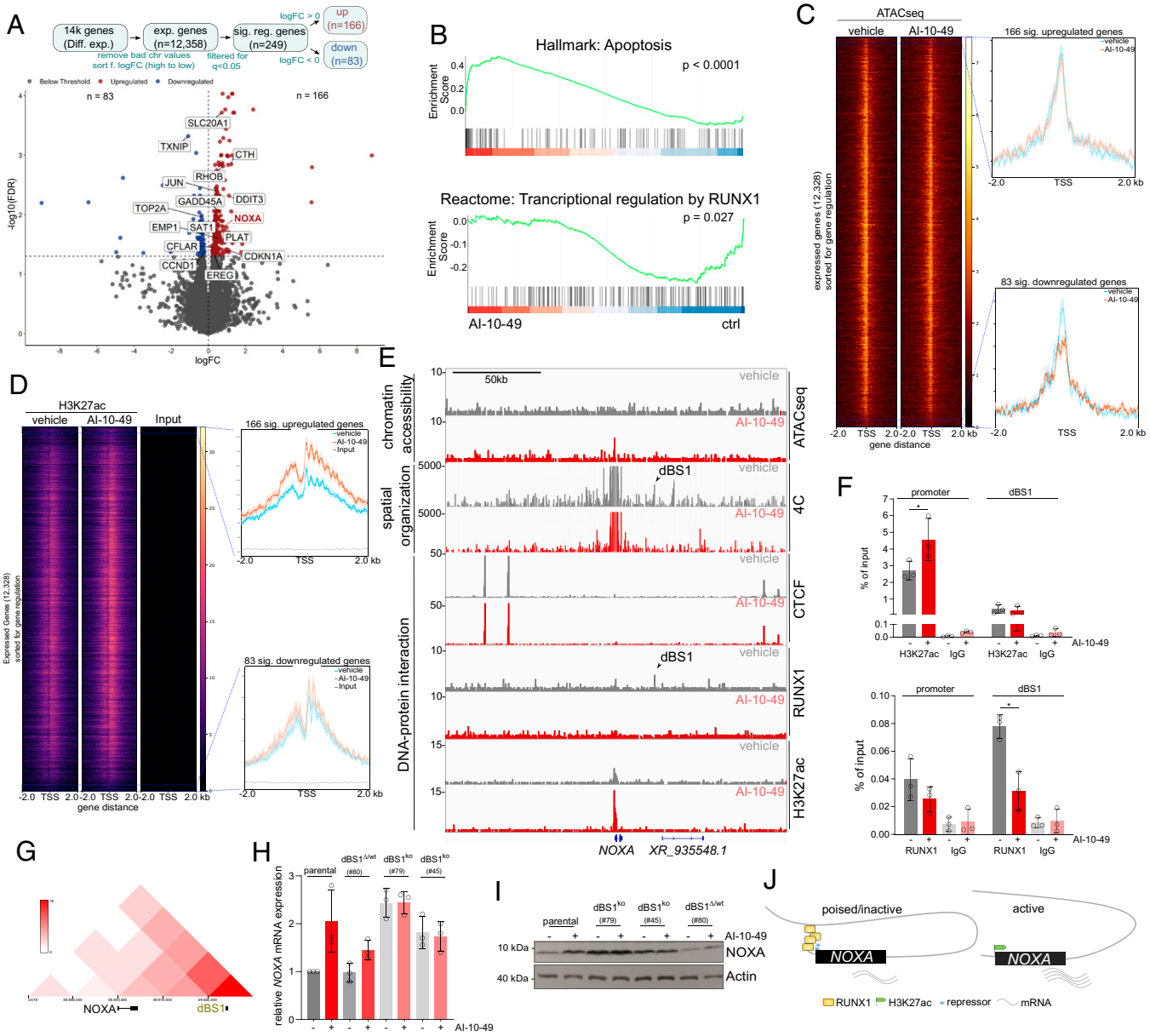

Fig. 3. RUNX1 inhibition induces a global redistribution of active chromatin and activates of the proximal promotor region of the NOXA gene. (*A*) (*Upper*) Sorting and filtering strategy to identify significantly up- and down-regulated genes. (*Lower*) Volcano plot of differential expressed genes. MiaPaCa-2 cells were treated with vehicle (DMSO) or AI-10-49 (3 μM) for 6 h ($n = 3$ biological replicates). (*B*) Indicated gene signatures of a GSEA from RNAseq data, described in *A*. (*C*) Heatmap representing open chromatin peaks of 12,328 expressed genes by omni-ATAC-seq analysis in DMSO- and AI-10-49–treated cells (3 μM for 6 h) ($n = 2$). Aggregate plots are of all significantly up- and down-regulated genes, identified in *A*. (*D*) Heatmap representing H3K27ac peaks in MiaPaCa-2 cells treated for 6 h with vehicle (DMSO) or 3 μM AI-10-49 ($n = 2$) and input. Aggregate plots display H3K27ac enrichment of all significantly up- and down-regulated genes, identified in *A*. (*E*) Omni-ATAC-seq (DNA accessibility) ($n = 2$), chromosome conformation capture (4C, spatial chromatin organization) ($n = 1$) and ChIPseq ($n = 2$) analysis for RUNX1, H3K27ac, and CTCF in vehicle (DMSO)- or AI-10-49–treated MiaPaCa-2 cells. Arrows indicate RUNX1 binding and an interaction of the *NOXA* gene at downstream binding site 1 (dBS1). (*F*) ChIP-qPCR analysis at the promoter and the downstream binding site 1 (dBS1) for RUNX1, H3K27ac, and IgG in DMSO- or AI-10-49–treated MiaPaCa-2 cells ($n = 3$). *t* test, $^*P < 0.05$. (*G*) Heatmap of Hi-C data from Panc1 cells generated by A.T.d.D. laboratory (36), accessed via http://3dgenome.fsm.northwestern.edu/, displaying spatial chromatin organization. (*H*) Relative *NOXA* mRNA expression in indicated clones of MiaPaCa-2 cells. The dBS1 binding site was excised using CRISPR-Cas9. Cells were treated for 6 h with 3 μM AI-10-49. (*I*) Western blot of NOXA 6 h after treatment with 3 μM AI-10-49 in indicated clones of MiaPaCa-2 cells. Actin served as loading control. (*J*) Schematic of RUNX1-mediated repression of the *NOXA* gene.

NOXA, subsequently leading to increased gene expression. To analyze the spatial organization of the *NOXA* region, we performed chromosome conformation capture assays (4C) to capture interactions between the *NOXA* locus (view point) and all other genomic loci. Here, we found a hitherto unknown interaction with a downstream region of the *NOXA* gene, which is abrogated upon AI-10-49 treatment and in *RUNX1*^{ko} cells (Fig. 3*E*, arrow/dBS1 and *SI Appendix*, Fig. S6*A*). Binding of the nuclear protein CCCTC-binding factor (CTCF), which marks insulator regions to prevent cross-talk between active and inactive chromatin, was unaffected (Fig. 3*E*). Additionally, RUNX1 peaks in the vehicle control (indicated by an arrow in Fig. 3*E*) and at the *NOXA* gene, arguing for a spatial interaction, which is mediated by RUNX1 (Fig. 3 *E* and *G*). The dBS1 region was

the only region within the CTCF boundaries where both RUNX1 binding and DNA–DNA interaction had disappeared after AI-10-49 treatment (Fig. 3*G* and *SI Appendix*, Fig. S6*A*). This spatial interaction could also be found in public Hi-C data of Panc1 (Fig. 3*F*) (36). Taken together, these data suggest that RUNX1 binding to the dBS1 region actively represses the *NOXA* gene. To identify which histone deacetylases are responsible for this effect, we used class I HDAC inhibitors. Here, in particular, inhibition of HDAC1/2 by Merck60 showed a significant induction of *NOXA* mRNA expression (*SI Appendix*, Fig. S6*B*) as well as an induction of the H3K27ac mark at the *NOXA* promoter (*SI Appendix*, Fig. S6*C*). Additionally, murine PDAC cells harboring a dual recombinase system and a 4-hydroxy-tamoxifen inducible Cre to knockout alleles for either *Hdac1* (PPT-F3641) or *Hdac2* (PPT-F1648) (*SI Appendix*, Fig. S6*D*) displayed a *Noxa* induction only in *Hdac2* deleted cells (*SI Appendix*, Fig. S6*E*), which is in line with a previous study showing that HDAC2 is responsible for the repression of *NOXA* in PDAC (11). Therefore, an HDAC2–RUNX1/CBFβ axis might be responsible for *NOXA* repression. This requires further validation.

To prove that the *dBS1* region is causative for the repression of *NOXA*, we first screened this region for evolutionary conserved *RUNX1* binding motifs, and, indeed, identified conserved RUNX1 consensus sequences (*SI Appendix*, Fig. S6*F*). We next performed a CRISPR-Cas9–mediated knockout of the *dBS1* region (*SI Appendix*, Fig. S6*G*) to genetically demonstrate its involvement in NOXA repression. Indeed, loss of the *dBS1* region led to increased *NOXA* mRNA (Fig. 3*H*) and protein levels (Fig. 3*I*). This demonstrates the repressive function of this RUNX1 binding site. In contrast to parental cells, AI-10-49 treatment did not further affect NOXA expression (Fig. 3 *H* and *I*). Furthermore, in the $dBS1^{\Delta/wt}$ clone, NOXA expression still was induced upon AI-10-49 treatment, albeit to a lesser extent (Fig. 3 *H* and *I*).

In summary, we describe a previously unknown mechanism of a RUNX1-mediated repression of the *NOXA* gene in PDAC. Through enrichment of an active chromatin mark at the *NOXA* gene itself, its expression is significantly increased (Fig. 3*J*), thereby inducing apoptosis. This mechanism could be crucial for therapeutic interventions that depend on a NOXA-induced cell death program.

RUNX1 Inhibition by AI-10-49 Is Effective In Vivo and in Patient-Derived Organoids. To validate whether RUNX1 inhibition could be effective in vivo, we first examined the efficacy of AI-10-49 in mice carrying MiaPaCa-2 PDAC xenografts (Fig. 4*A*). AI-10-49 treatment resulted in a significant decrease in tumor volume (Fig. 4*B*) and proliferative capacity (Ki67, Fig. 4*C*). Importantly, AI-10-49 treatment induced apoptosis measured by cleaved caspase 3 (CC3) positivity in the tumor compared to the vehicle control in parental cells (Fig. 4 *B* and *C*). Whereas parental cells did not change in tumor volume after AI-10-49 treatment, $NOXA^{ko}$ cells still grew upon treatment, supporting NOXA as an essential contributor of AI-10-49 efficacy (Fig. 4*B*). Additionally, no significant difference between control and treatment was observed in either K67 or CC3 stainings in $NOXA^{ko}$ cells (Fig. 4*D*). Taken together, these data indicate that apoptosis induction by AI-10-49 treatment is also dependent on NOXA in vivo.

We next isolated seven human patient-derived organoids (PDOs) from PDAC patients to investigate RUNX1 inhibition by AI-10-49. First, we performed transcriptome profiling (*SI Appendix*, Table S5), and sorted PDOs for high and low *NOXA* mRNA expression (Fig. 4*E*). Gene set enrichment analysis revealed a significant ($q < 0.001$) accumulation of an apoptosis signature in the PDOs with a high *NOXA* expression (Fig. 4*F*). PDOs with a high *NOXA* expression showed the strongest growth inhibition toward AI-10-49 treatment, which further supports our previous findings (Fig. 4*G*).

Overall, these findings show that RUNX1 inhibition might be a therapeutic option to treat PDAC.

Discussion

Molecular tumor profiling and functional studies have led to the identification and validation of genes and signaling pathways that are dysregulated or mutated in PDAC (7, 37–39). Based on comprehensive molecular characterization of PDACs (6–9), it might thus be possible to define personalized treatment strategies (38). An imbalance of signaling pathways, such as cell death–associated pathways, promotes tumor maintenance and treatment resistance in PDAC (3). In this study, we analyzed publicly available transcriptome profiles of PDAC patients and found that increased *NOXA* mRNA expression defines an aggressive squamous/QM subtype. In contrast to NOXA, which is tightly regulated at the transcriptional level in PDAC (11), one of its antiapoptotic counterparts, MCL1 (10), is mostly regulated at the protein level (40). Since *NOXA* mRNA and protein expression do not correlate strongly, as has been shown in mantle cell lymphoma (41) and in PDAC (11), it is important to identify substances that can induce apoptosis by taking advantage of a NOXA-associated vulnerability. We therefore performed drug-screening experiments in isogenic cell models with *NOXA*-deficient and *NOXA*-proficient counterparts to search for compounds that can exploit this vulnerability. We unexpectedly found a substance that inhibits the core binding alpha units RUNX1, RUNX2, or RUNX3 with CBFβ.

The functions of RUNX1 are highly specific, depending on the tissue and cell type. Deletion of *Runx1* in a mouse model of T cell acute lymphoblastic leukemia (T-ALL) (42), silencing of *RUNX1* in human T-ALL cells (42), and silencing of *RUNX1* in SW480 human colon cancer cells (43) all triggered apoptosis. In contrast, in Kasumi-1 *t* (8, 21) leukemia cells, RUNX1 overexpression induced apoptosis by eliciting expression of the cyclin-dependent kinase inhibitor $p57^{Kip2}$ (44). In line with the biological effects observed in T-ALL (42) and in colon cancer cells (43), we observed an induction of apoptosis both through the pharmacological CBFβ/RUNX1 inhibition by the compound AI-10-49 and in CRISPR-Cas9–mediated knockouts of *RUNX1*. We observed a significant induction of *NOXA* mRNA expression, which was exclusive to *RUNX1* knockout cells and could not be observed in *RUNX2* or *RUNX3* knockout cells, arguing for a nonredundant function for RUNX1.

In a chemical high-throughput screen, which was performed to identify compounds that disrupt the interaction between RUNX1 and the CBFβ-MYH11/SMMHC fusion protein, first, a lead molecule was identified, which exhibited low selectivity for the fusion protein (33). Therefore, a bivalent derivate of this compound was generated. AI-10-49 inhibits CBFβ-MYH11/SMMHC with an increased selectivity and restores the formation of wild-type CBFβ-RUNX1 (33). In cells lacking the CBFβ-MYH11/SMMHC fusion protein, AI-10-49 acts like the monomeric lead molecule and inhibits wild-type CBFβ/RUNX1. In fact, AI-10-49 treatment as a putative pharmacological CBFβ/RUNX1 inhibitor, as well as a genetic knockout of *RUNX1*, unexpectedly showed an induction of NOXA, similarities in transcriptional regulation at a genome-wide scale, and an associated apoptosis induction in PDAC cells, arguing for RUNX1 as a repressor of *NOXA* gene expression. We could show that the pharmacological CBFβ/RUNX1 inhibition leads to a global enrichment of H3K27ac, a marker for active chromatin, including the *NOXA* gene. We observed an unexpected punctual interaction of a NOXA downstream RUNX1 binding site and the NOXA promoter. How exactly RUNX1 exercises its repressive function in PDAC has to be addressed in detail in further studies. An analysis of different datasets showed a high expression of RUNX1 in pancreatic cancer compared to

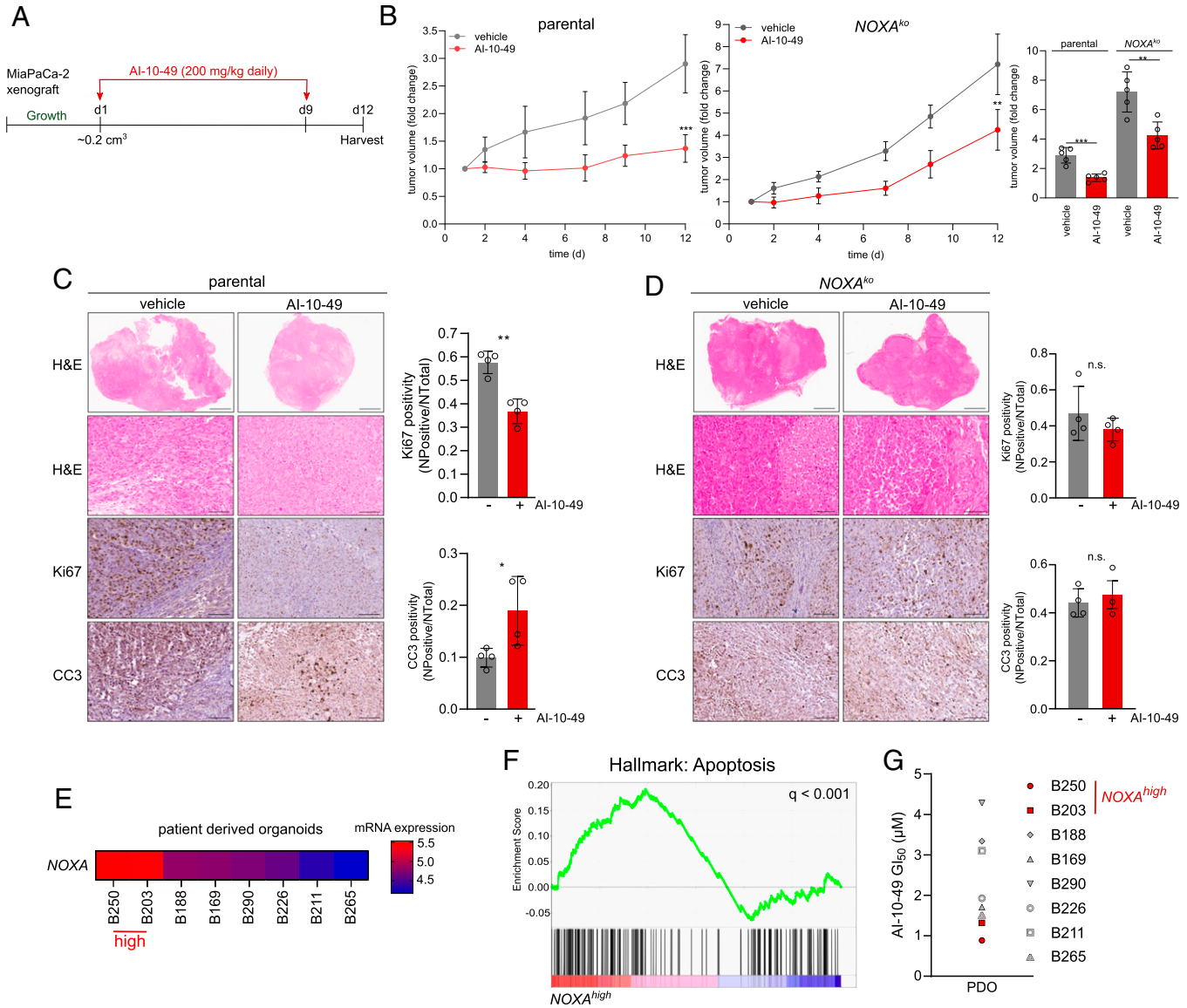

Fig. 4. Tumor growth is blocked by RUNX1 inhibition in vivo and in PDOs. (*A*) Mice were treated with 200 mg/kg AI-10-49 intraperitoneally daily for 9 d. Treatment started (d1) when tumors reached a volume of 0.2 cm^3. (*B*) Tumor size was measured over time in parental and *NOXA*^{ko} xenografts. AI-10-49–treated mice showed a significant tumor growth inhibition ($n = 5$ mice in each group).$^{**}P < 0.01$, $^{***}P < 0.001$ (Student's *t* test). (*C*) IHC of parental xenografts. (*Left*) Representative pictures of tumors from AI-10-49 and vehicle-treated mice. Displayed are full scans of the tumors. (Scale bar, 2 mm); detailed pictures of H&E stained and IHC for Ki67 and CC3. (Scale bar, 100 μm.) (*Right*) Quantification of Ki67 and CC3 IHC staining of AI-10-49–treated tumor xenografts using the Aperio positive pixel method. $^{*}P < 0.055$, $^{**}P < 0.01$ (*t* test). (*D*) IHC of *NOXA*^{ko} xenografts as indicated in *C*. n.s.: not significant (*t* test); Scale bar, 2 mm. (*E*) RNAseq data of seven PDOs were analyzed for *NOXA* expression. *NOXA* mRNA expression > 75% = *NOXA*^{high}; NOXA mRNA expression < 25% = *NOXA*^{low}. (*F*) GSEA of RNAseq data of PDOs; hallmark apoptosis signature in the *NOXA*^{high} subtype. Nominal *P* value < 0.001. FDR-q value is depicted. (*G*) Dose–response treatment of PDOs viability measured 72 h after AI-10-49 treatment with CellTiterGlo.

normal pancreas. Of note is that knockdown of *RUNX1* in PDAC cells was shown to suppress the invasive/aggressive phenotype via regulation of miR-93 (45). In particular, high RUNX1 expression and RUNX1 target gene signatures were observed in premalignant Kras^{G12D}-driven murine pancreatic epithelial cells, which, together, indicate a largely unexplored and possibly unexploited relevance of RUNX1 in PDAC.

Since the apoptosis machinery in PDAC cells retains its functionality (3), the strategy of directly inhibiting prosurvival BCL2 proteins such as the NOXA antagonist MCL1 appears extremely attractive (46). One of the first selective MCL1 inhibitors with in vivo activity, S63845, showed massive apoptosis induction in multiple myeloma and acute myeloid leukemia, but many solid tumors were resistant to S63845 monotherapy (47). Combination therapies such as S63845 with the SRC kinase inhibitor Dasatinib reduced cell viability in PDAC models and even led to a reduction in metastasis formation (48). These data show that the development of new therapeutic strategies, especially with regard to apoptosis evasion for PDAC, is extremely promising in improving the current clinical regimens. Whether compounds like S63845 synergistically combine with AI-10-49 is currently under investigation.

Unraveling the transcriptional regulation of apoptosis-associated genes and the interplay of transcription factors, such as RUNX1, is important to understand the tumor biology of PDAC. The development and improvement of compounds that can inhibit transcription factors, such as the CBFβ/RUNX1 inhibitor used here, perhaps in combination with proteolysis-targeting chimeras technology (49), could provide new

approaches for PDAC treatment. Therefore, our mechanistic work, demonstrating a control of NOXA by a repressive facet of RUNX1, opens a research direction into potent RUNX1 inhibitors and a way to target this deadly disease.

Data Availability. RNA-Sequencing (cell lines), Chromatin Immunoprecipitation DNA-Sequencing, Assay for Transposase-Accessible Chromatin using sequencing, and Chromosome conformation capture-on-chip data are publicly available and have been deposited in the European Nucleotide Archive (ENA). The data can be accessed via the website https://www.ebi.ac.uk/ under accession no. PRJEB39828. RNAseq (organoids) gene expression matrix is shown in *SI Appendix*, Table S5. In addition, transcriptome data and chromatin immunoprecipitation DNA sequencing from studies in references 53, 54, 55, and 56 were used.

ACKNOWLEDGMENTS. We thank Martin Schlensog and Yakup Yasar for performing the IHC staining. We thank Dieter Saur for providing murine PDAC cell lines, and thank Ernesto Acevedo for providing the p53(1C12) antibody. This study was conducted with the support of the Ontario Institute for Cancer Research through funding provided by the Government of Ontario. Funding was provided by Else-Kröner-Fresenius Stiftung (Grant 2016_A43) to M.W.; Walter Schulz Stiftung to M.W.; Deutsche Forschungsgemeinschaft SFB 1321 Project C13 (Project ID 329628492) to G.S., SCHN 959/6-1 and SCHN 959/3-2 to G.S., and SFB 1335 Project P3 (Project ID 360372040) to U.K.; Wilhelm-Sander-Stiftung (Grant 2017.048.2) to G.S. and U.K.; Deutsche Krebshilfe Project 70114425 to U.K.; Stiftung Charité to U.K.; European Research Council (TarMYC) to E.W.; Wilhelm Sander Foundation (Grant 2019.086), Brigitte und Dr. Konstanze Wegener-Stiftung (Project 65), Deutsche Forschungsgemeinschaft (DFG, German Research Foundation) – Project-ID 393547839 – SFB 1361 and Projects KR2291/9-1/12-1/14-1 to O.H.K.

1. R. L. Siegel, K. D. Miller, A. Jemal, Cancer statistics, 2020. *CA Cancer J. Clin.* **70**, 7–30 (2020).
2. D. Hanahan, R. A. Weinberg, Hallmarks of cancer: The next generation. *Cell* **144**, 646–674 (2011).
3. R. Hamacher, R. M. Schmid, D. Saur, G. Schneider, Apoptotic pathways in pancreatic ductal adenocarcinoma. *Mol. Cancer* **7**, 64 (2008).
4. J. E. Bradner, D. Hnisz, R. A. Young, Transcriptional addiction in cancer. *Cell* **168**, 629–643 (2017).
5. Y. Cheng *et al.*, Targeting epigenetic regulators for cancer therapy: Mechanisms and advances in clinical trials. *Signal Transduct. Target. Ther.* **4**, 62 (2019).
6. P. Bailey *et al.*, Australian Pancreatic Cancer Genome Initiative, Genomic analyses identify molecular subtypes of pancreatic cancer. *Nature* **531**, 47–52 (2016).
7. E. A. Collisson, P. Bailey, D. K. Chang, A. V. Biankin, Molecular subtypes of pancreatic cancer. *Nat. Rev. Gastroenterol. Hepatol.* **16**, 207–220 (2019).
8. E. A. Collisson *et al.*, Subtypes of pancreatic ductal adenocarcinoma and their differing responses to therapy. *Nat. Med.* **17**, 500–503 (2011).
9. R. A. Moffitt *et al.*, Virtual microdissection identifies distinct tumor- and stroma-specific subtypes of pancreatic ductal adenocarcinoma. *Nat. Genet.* **47**, 1168–1178 (2015).
10. A. Strasser, S. Cory, J. M. Adams, Deciphering the rules of programmed cell death to improve therapy of cancer and other diseases. *EMBO J.* **30**, 3667–3683 (2011).
11. P. Fritsche *et al.*, HDAC2 mediates therapeutic resistance of pancreatic cancer cells via the BH3-only protein NOXA. *Gut* **58**, 1399–1409 (2009).
12. M. Wirth *et al.*, MYC and EGR1 synergize to trigger tumor cell death by controlling NOXA and BIM transcription upon treatment with the proteasome inhibitor bortezomib. *Nucleic Acids Res.* **42**, 10433–10447 (2014).
13. K. Lankes *et al.*, Targeting the ubiquitin-proteasome system in a pancreatic cancer subtype with hyperactive MYC. *Mol. Oncol.* **14**, 3048–3064 (2020).
14. E. Oda *et al.*, Noxa, a BH3-only member of the Bcl-2 family and candidate mediator of p53-induced apoptosis. *Science* **288**, 1053–1058 (2000).
15. C. Ploner, R. Kofler, A. Villunger, Noxa: At the tip of the balance between life and death. *Oncogene* **27**, S84–S92 (2008).
16. L. S. Chuang, K. Ito, Y. Ito, RUNX family: Regulation and diversification of roles through interacting proteins. *Int. J. Cancer* **132**, 1260–1271 (2013).
17. B. A. Otálora-Otálora, B. Henríquez, L. López-Kleine, A. Rojas, RUNX family: Oncogenes or tumor suppressors (Review). *Oncol. Rep.* **42**, 3–19 (2019).
18. M. Ichikawa *et al.*, AML-1 is required for megakaryocytic maturation and lymphocytic differentiation, but not for maintenance of hematopoietic stem cells in adult hematopoiesis. *Nat. Med.* **10**, 299–304 (2004).
19. Y. Lou *et al.*, A Runx2 threshold for the cleidocranial dysplasia phenotype. *Hum. Mol. Genet.* **18**, 556–568 (2009).
20. H. Fukamachi, K. Ito, Growth regulation of gastric epithelial cells by Runx3. *Oncogene* **23**, 4330–4335 (2004).
21. K. Inoue *et al.*, Runx3 controls the axonal projection of proprioceptive dorsal root ganglion neurons. *Nat. Neurosci.* **5**, 946–954 (2002).
22. R. Mevel, J. E. Draper, M. Lie-A-Ling, V. Kouskoff, G. Lacaud, RUNX transcription factors: Orchestrators of development. *Development* **146**, dev148296 (2019).
23. M. Uhlen *et al.*, A pathology atlas of the human cancer transcriptome. *Science* **357**, eaan2507 (2017).
24. K. Shigesada, B. van de Sluis, P. P. Liu, Mechanism of leukemogenesis by the inv(16) chimeric gene CBFB/PEBP2B-MHY11. *Oncogene* **23**, 4297–4307 (2004).
25. C. J. Scheitz, T. S. Lee, D. J. McDermitt, T. Tumbar, Defining a tissue stem cell-driven Runx1/Stat3 signalling axis in epithelial cancer. *EMBO J.* **31**, 4124–4139 (2012).
26. D. J. Birnbaum *et al.*, Expression of genes with copy number alterations and survival of patients with pancreatic adenocarcinoma. *Cancer Genomics Proteomics* **13**, 191–200 (2016).
27. C. J. Scheitz, T. Tumbar, New insights into the role of Runx1 in epithelial stem cell biology and pathology. *J. Cell. Biochem.* **114**, 985–993 (2013).
28. I. Kitabayashi, A. Yokoyama, K. Shimizu, M. Ohki, Interaction and functional cooperation of the leukemia-associated factors AML1 and p300 in myeloid cell differentiation. *EMBO J.* **17**, 2994–3004 (1998).
29. X. Zhao *et al.*, Methylation of RUNX1 by PRMT1 abrogates SIN3A binding and potentiates its transcriptional activity. *Genes Dev.* **22**, 640–653 (2008).
30. Z. Sheng, S. Z. Wang, M. R. Green, Transcription and signalling pathways involved in BCR-ABL-mediated misregulation of 24p3 and 24p3R. *EMBO J.* **28**, 866–876 (2009).
31. M. Chan-Seng-Yue *et al.*, Transcription phenotypes of pancreatic cancer are driven by genomic events during tumor evolution. *Nat. Genet.* **52**, 231–240 (2020).
32. J. A. Pulikkan *et al.*, CBFβ-SMMHC inhibition triggers apoptosis by disrupting MYC chromatin dynamics in acute myeloid leukemia. *Cell* **174**, 172–186.e21 (2018).
33. A. Illendula *et al.*, Chemical biology. A small-molecule inhibitor of the aberrant transcription factor CBFβ-SMMHC delays leukemia in mice. *Science* **347**, 779–784 (2015).
34. D. Gfeller *et al.*, SwissTargetPrediction: A web server for target prediction of bioactive small molecules. *Nucleic Acids Res.* **42**, W32–W38 (2014).
35. D. Wu, T. Ozaki, Y. Yoshihara, N. Kubo, A. Nakagawara, Runt-related transcription factor 1 (RUNX1) stimulates tumor suppressor p53 protein in response to DNA damage through complex formation and acetylation. *J. Biol. Chem.* **288**, 1353–1364 (2013).
36. ENCODE Project Consortium, An integrated encyclopedia of DNA elements in the human genome. *Nature* **489**, 57–74 (2012).
37. M. Orth *et al.*, Pancreatic ductal adenocarcinoma: Biological hallmarks, current status, and future perspectives of combined modality treatment approaches. *Radiat. Oncol.* **14**, 141 (2019).
38. C. Torres, P. J. Grippo, Pancreatic cancer subtypes: A roadmap for precision medicine. *Ann. Med.* **50**, 277–287 (2018).
39. A. Biederstädt *et al.*, SUMO pathway inhibition targets an aggressive pancreatic cancer subtype. *Gut* **69**, 1472–1482 (2020).
40. R. M. Fritsch, G. Schneider, D. Saur, M. Scheibel, R. M. Schmid, Translational repression of MCL-1 couples stress-induced eIF2 alpha phosphorylation to mitochondrial apoptosis initiation. *J. Biol. Chem.* **282**, 22551–22562 (2007).
41. M. A. Dengler *et al.*, Discrepant NOXA (PMAIP1) transcript and NOXA protein levels: A potential Achilles' heel in mantle cell lymphoma. *Cell Death Dis.* **5**, e1013 (2014).
42. A. Choi *et al.*, RUNX1 is required for oncogenic Myb and Myc enhancer activity in T-cell acute lymphoblastic leukemia. *Blood* **130**, 1722–1733 (2017).
43. Y. Zhou *et al.*, LRG1 promotes proliferation and inhibits apoptosis in colorectal cancer cells via RUNX1 activation. *PLoS One* **12**, e0175122 (2017).
44. S. Liu *et al.*, RUNX1 inhibits proliferation and induces apoptosis of t(8;21) leukemia cells via KLF4-mediated transactivation of P57. *Haematologica* **104**, 1597–1607 (2019).
45. Y. Cheng *et al.*, RUNX1 promote invasiveness in pancreatic ductal adenocarcinoma through regulating miR-93. *Oncotarget* **8**, 99567–99579 (2017).
46. S. H. Wei *et al.*, Inducing apoptosis and enhancing chemosensitivity to gemcitabine via RNA interference targeting Mcl-1 gene in pancreatic carcinoma cell. *Cancer Chemother. Pharmacol.* **62**, 1055–1064 (2008).
47. A. Kotschy *et al.*, The MCL1 inhibitor S63845 is tolerable and effective in diverse cancer models. *Nature* **538**, 477–482 (2016).
48. L. Castillo *et al.*, Australian Pancreatic Cancer Genome Initiative (APGI), MCL-1 antagonism enhances the anti-invasive effects of dasatinib in pancreatic adenocarcinoma. *Oncogene* **39**, 1821–1829 (2020).
49. X. Sun *et al.*, PROTACs: Great opportunities for academia and industry. *Signal Transduct. Target. Ther.* **4**, 64 (2019).
50. C. D. Logsdon *et al.*, Molecular profiling of pancreatic adenocarcinoma and chronic pancreatitis identifies multiple genes differentially regulated in pancreatic cancer. *Cancer Res.* **63**, 2649–2657 (2003).
51. M. Uhlén *et al.*, Proteomics. Tissue-based map of the human proteome. *Science* **347**, 1260419 (2015).
52. D. Alonso-Curbelo *et al.*, A gene-environment-induced epigenetic program initiates tumorigenesis. *Nature* **590**, 642–648 (2021).
53. L. Badea, V. Herlea, S. O. Dima, T. Dumitrascu, I. Popescu, Combined gene expression analysis of whole-tissue and microdissected pancreatic ductal adenocarcinoma identifies genes specifically overexpressed in tumor epithelia. *Hepatogastroenterology* **55**, 2016–2027 (2008).
54. H. Pei *et al.*, FKBP51 affects cancer cell response to chemotherapy by negatively regulating Akt. *Cancer Cell.* **16**, 259–266 (2009).
55. J. T. Rose *et al.*, Inhibition of the RUNX1-CBFβ transcription factor complex compromises mammary epithelial cell identity: a phenotype potentially stabilized by mitotic gene bookmarking. *Oncotarget* **11**, 2512–2530 (2020).
56. E. P. Consortium, An integrated encyclopedia of DNA elements in the human genome. *Nature* **489**, 57–74 (2012).